catalysts

MDPI

Article

Hierarchically-Structured TiO_2/MnO_2 Hollow Spheres Exhibiting the Complete Mineralization of Phenol

Caiguo Jiang [1], Yi Ge [2], Wenjing Chen [1], Li Hua [3], Huiquan Li [4,*], Ying Zhang [1,4] and Shunsheng Cao [1,4,*]

1 Research Institute of Polymer Materials, School of Materials Science and Engineering, Jiangsu University, Zhenjiang 212013, China; 2211605015@stmail.ujs.edu.cn (C.J.); cwjing1996@126.com (W.C.); qiushuiyiren2024@126.com (Y.Z.)
2 Pharmaceutical Science/Biotechnology, School of Pharmacy/CMU-QUB Joint College, Queen's University Belfast, 97 Lisburn Road, Belfast BT9 7BL, UK; y.ge@qub.ac.uk
3 College of Chemical Engineering, Yangzhou Polytechnic Institute, Yangzhou 225127, China; huali795@sohu.com
4 Anhui Provincial Key Laboratory for Degradation and Monitoring of the Pollution of the Environment, School of Chemistry & Materials Engineering, Fuyang Normal College, Qinghe West Road 100, Fuyang 236037, China
* Correspondence: huiquanli0908@163.com (H.L.); sscao@ujs.edu.cn (S.C.)

Received: 19 March 2019; Accepted: 13 April 2019; Published: 25 April 2019

Abstract: Although TiO_2 or MnO_2-based materials have been widely used for the degradation of phenolic compounds, complete mineralization is still a challenge, especially for TiO_2-based materials. Here, we devise a hierarchically-structured TiO_2/MnO_2 (HTM) hollow sphere, in which hollow TiO_2 acts as a skeleton for the deposition of MnO_2 in order to prevent the aggregation of MnO_2 nanoparticles and to maintain its hollow structure. During the oxidation reaction, the as-synthesized HTM can fully exert their respective advantages of the TiO_2 and MnO_2 species to realize the first stage of the rapid oxidation degradation of phenol and the second stage of the complete photo-mineralization of residual phenol and its intermediates, which efficiently overcomes the incomplete mineralization of phenolic compounds. The degradation mechanism and pathway of phenol are also proposed according to the analysis of Mass Spectrometry (MS). Therefore, this work provides a new insight for exploring hierarchically-structured materials with two or more species.

Keywords: hierarchically-structured TiO_2/MnO_2; chemical oxidation degradation; photo-mineralization; phenol

1. Introduction

As one of the persistent organic pollutants in surface water sources, phenol and its derivatives are widely used as raw materials in many chemical, petrochemical, and pharmaceutical fields [1,2]. Clearly, the continuous addition of phenolic compounds to the environment has led to a significantly enhanced toxic contamination because they are hard to be decomposed even at low concentrations [3,4]. Therefore, effective strategies for completely removing phenolic compounds from wastewater are urgently required.

Membrane-based separation methods are widely used for wastewater treatment because of the good performance of the reverse osmosis and nanofiltration process [5,6]. However, the method often shows a low retention of many organic micropollutants and suffers from severe fouling problems. By contrast, considerable efforts have been focused on the design of TiO_2-based photocatalysts for the

removal of phenolic compounds [7,8] due to their powerful oxidizing ability, chemical stability, and low cost [9–11]. For example, Makrigianni et al. [12] confirmed that pure TiO_2 could only remove 65% of phenol within five hours under simulated natural sunlight irradiation. Wang et al. [13] prepared a composite hollow TiO_2 photocatalyst and found that it degraded 73% of phenol under sunlight irradiation after 4 h. Zheng et al. [14] synthesized electrochromic titania nanotube arrays and removed 78.2% of phenol after 3 h under simulated sunlight irradiation. Unfortunately, an efficient method for the complete degradation of phenolic compounds is extremely difficult for TiO_2-based photocatalysts even under simulated sunlight irradiation [15,16]. Accordingly, the design of novel and efficient degradation systems that can mineralize phenol completely is highly desirable.

Many studies have proven that manganese dioxide (MnO_2) can produce sulfate radicals (SO^{4-}) by activating peroxomonosulfate (PMS) [17–20], achieving the effective degradation of phenolic compounds [21,22]. Liang et al. [23] reported that mesoporous Co_3O_4/MnO_2 material manifested a 100% phenol removal rate within 100 min. Wang et al. [2] found that a 3D structure of corolla-like MnO_2 could obtain a 100% phenol removal rate. Edy et al. [24] devised one-dimensional MnO_2 nanowires and demonstrated that as-synthesized α-MnO_2 exhibited 100% phenol degradation. In many cases, however, the amount of total organic carbon was still not negligible even if the complete degradation of phenol was obtained according to the detection of high-performance liquid chromatography (HPLC) [2,19,23,25].

Based on the above considerations, we devise a hierarchically-structured TiO_2/MnO_2 (HTM) for the first time, in which the outer MnO_2 can achieve the fast and efficient oxidation of phenol by activating PMS, while the inner TiO_2 not only acts as a skeleton to sustain MnO_2, but also further mineralizes a small amount of undegraded phenol and intermediates under simulated sunlight irradiation. Composites comprised of two metal oxides possess improved physicochemical properties compared to the use of pure oxides [26]. Moreover, the hollow/porous nature of the HTM boosts the diffusion of reactants by lowering diffusion resistance [27]. More importantly, the HTM can fully exert their respective advantages in the TiO_2 and MnO_2 species, realizing the first stage of chemical oxidation degradation and the second stage of complete photo-mineralization. Therefore, the as-synthesized HTM manifests the complete mineralization of phenol, efficiently overcoming the respective disadvantages of TiO_2 and MnO_2 for the incomplete mineralization of phenolic compounds in wastewater. This work provides a new insight for constructing hierarchically-structured materials with two or more species.

2. Results and Discussion

2.1. The Preparation and Structure of TiO_2/MnO_2 (HTM) Spheres

HTM hollow spheres were prepared via several steps: Firstly, a CPS@TiO_2 composite was synthesized by referring our previous works [9,10,28]. Secondly, TiO_2 hollow spheres could be achieved after calcination at 450 °C. Thirdly, the resulting TiO_2 hollow spheres were used as templates for the deposition of manganese nitrate due to the electrostatic interactions. Finally, the TiO_2/MnO_2 (HTM) was formed through calcination at 450 °C.

Figure 1 indicates the TEM and SEM images of hollow TiO_2 and HTM spheres. Compared with TiO_2 hollow spheres (average size: 510 ± 10 nm) (Figure 1a), each HTM hollow sphere has a thicker shell (average size: 523 ± 15 nm), suggesting a successful deposition of manganese dioxide. More importantly; some crystalline floccules located on the outer surface of the HTM can be clearly observed (Figure 1b), which are further confirmed by the SEM image of the HTM (Figure 1d). Unlike the smooth surface of hollow TiO_2 spheres (Figure 1c), the surface of the HTM hollow spheres become rougher due to the existence of many small crystalline MnO_2 nanoparticles (Figure 1d), further confirming the successful loading of manganese dioxide. The hollow structure of TiO_2/MnO_2 is ascertained by a STEM mapping measurement. As shown in Figure 2, energy dispersive x-ray (EDX) spectral region exhibits clear signals of O, Mn and Ti elements in the HTM sample, indicating the presence of MnO_2

and TiO_2. Figure 2d indicates that the Ti signal keeps the shape of the sphere, which fairly agrees with the results measured by the SEM and TEM. Interestingly, the Mn signal (Figure 2e) is mostly dispersed throughout the HTM spheres, forming a sphere similar to the Ti signal. EDX mapping results confirm that MnO_2 has been homogeneously anchored on the surface of the hollow TiO_2 spheres.

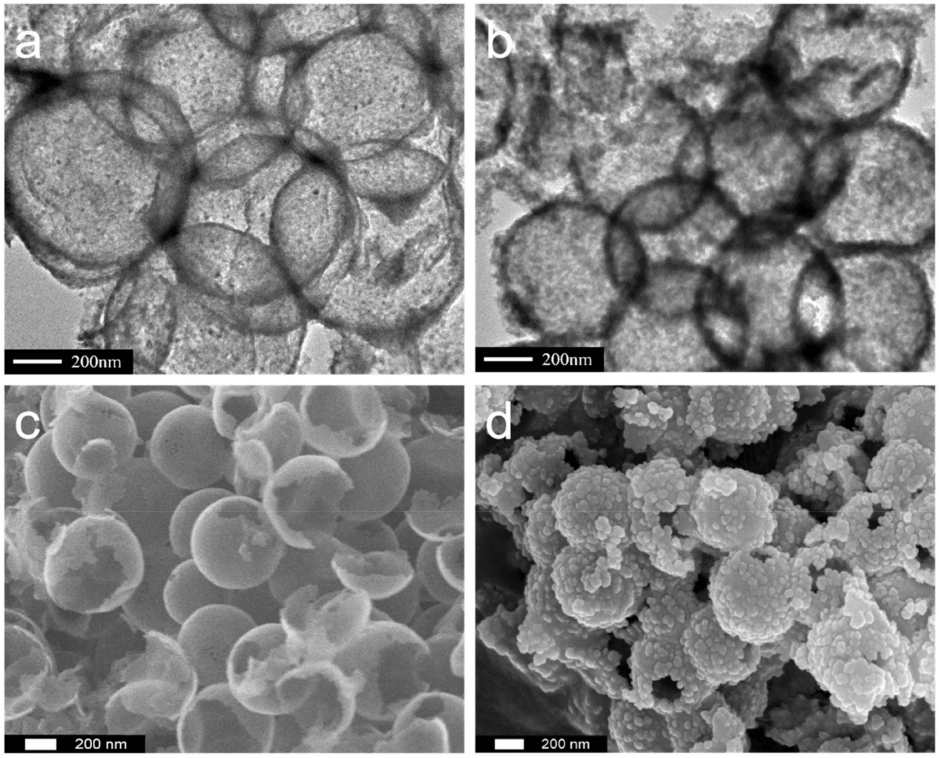

Figure 1. TEM and SEM images of hollow TiO_2 spheres (**a**,**c**) and HTM spheres (**b**,**d**).

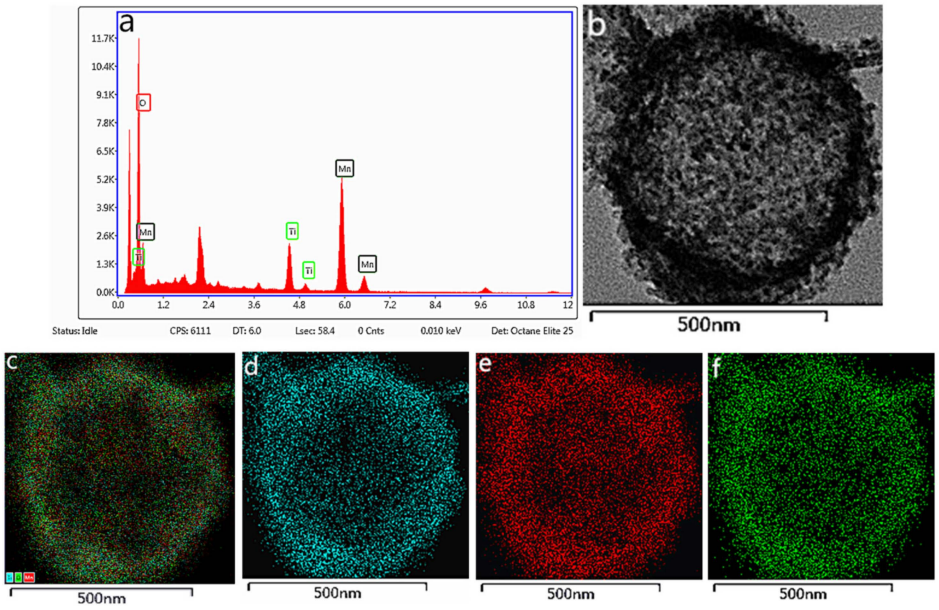

Figure 2. EDX spectrum of areas (**a**), SEM (**b**), STEM image (**c**) and EDX mapping of HTM (**d**) Ti, (**e**) Mn, and (**f**) O.

Figure 3 shows that the HTM exhibits a representative type IV curve with a clear hysteresis loop [29,30], which is clearly different from the porous/hollow TiO_2 spheres [31] (Figure 3a) with a high

surface area (~90.2283 m^2/g). By contrast, the capillary condensation of the HTM in N_2 adsorption and desorption is completely ascribed to the formation of MnO_2 particles on the surface of the porous/hollow TiO_2, leading to a decreased surface area (53.7827 m^2/g). In addition, thermogravimetric measurement of the HTM shows that only a 5.69% mass loss is observed between 100 and 450 °C (Figure S1), indicating that the HTM sample has a good structural stability and a low carbon amount in the HTM spheres. This is further confirmed by Raman spectra because no significant peaks are found to be attributed to the D-bands and G-bands of carbon materials (Figure S2) [32]. All these results strongly confirm that the hierarchical TiO_2/MnO_2 hollow spheres have been successfully prepared.

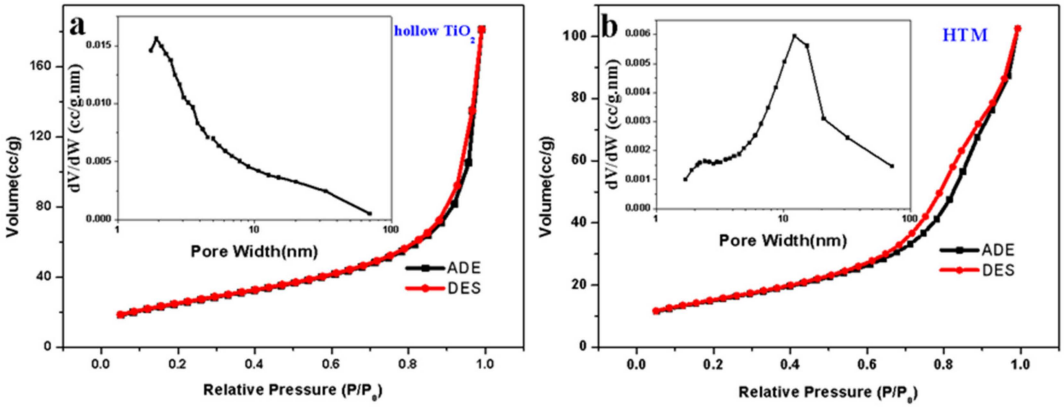

Figure 3. N_2 adsorption-desorption isotherms and pore size distribution (insert) of hollow TiO_2 (**a**) and HTM hollow spheres (**b**).

2.2. Crystal Structure and Bonding Environment of HTM Spheres

Figure 4 shows that the identified peaks of the HTM can be clearly attributed to anatase TiO_2 (JCPDS: 21-1272) [33,34], while four distinctive MnO_2 reflection peaks at 37.12° (100), 42.4° (101), 56.03°(102), 66.76° (110) are in line with the standard spectrum for MnO_2 (JCPDS: 30-0820) [35,36]. In addition, some weak peaks from $MnTiO_3$ are seen. According to the Scherrer equation ($D = \frac{k\lambda}{\beta \cos \theta}$), the crystallite size of TiO_2 is ~3.7 nm resulting from XRD, while the crystallite size of MnO_2 is ~11.96 nm. The well-defined diffraction rings in the selected electron area diffraction (SEAD) can be indexed as (100), (101), (102), (110) planes of MnO_2 (Figure S3), which is consistent with the XRD results. The XRD results show the formation of manganese dioxide and a small amount of MnO_2 doping in the HTM spheres [37].

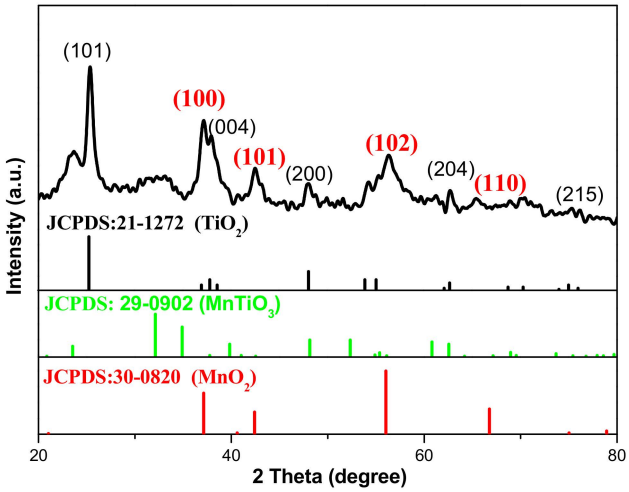

Figure 4. XRD patterns of TiO_2/MnO_2 and standard XRD patterns of anatase and manganese dioxide.

XPS analysis is used to obtain the chemical state and bonding environment of HTM, helping us understand basic information about the interaction between TiO_2 and MnO_2. As shown in Figure 5a, the elements of C, Ti, O and Mn can be evidently seen according to the binding energies of C1s, Ti2p, O1s and Mn2p, which fairly agrees with the measurement in the EDX spectral region (Figure 2a). In the case of the Ti2p, Figure 5b shows that the peak at 464.4 eV is attributed to $Ti2p_{1/2}$, and the other peak at 458.75 eV is indexed to $Ti2p_{3/2}$. The positive shift (~0.2 eV) of $Ti2p_{3/2}$ and (~0.17 eV) of $Ti2p_{1/2}$ can be observed for the HTM compared with the corresponding binding energies of hollow TiO_2 spheres (HT) (458.55 eV and 464.23 eV) [31]. The increases in the binding energies may be ascribed to the combined actions between MnO_2, carbon and host TiO_2. In detail, the Ti2p peak of HTM can be resolved into two Gaussian peaks, as demonstrated in Figure 5c. The peaks at 464.84 and 459.05 eV can be indexed to the $Ti2p_{1/2}$ and $Ti2p_{3/2}$ core levels of Ti^{4+}, respectively. While two peaks located at 463.62 and 458.05 eV are ascribed to the $Ti2p_{1/2}$ and $Ti2p_{3/2}$ peaks of Ti^{3+}, respectively, revealing the existence of oxygen vacancies [38].

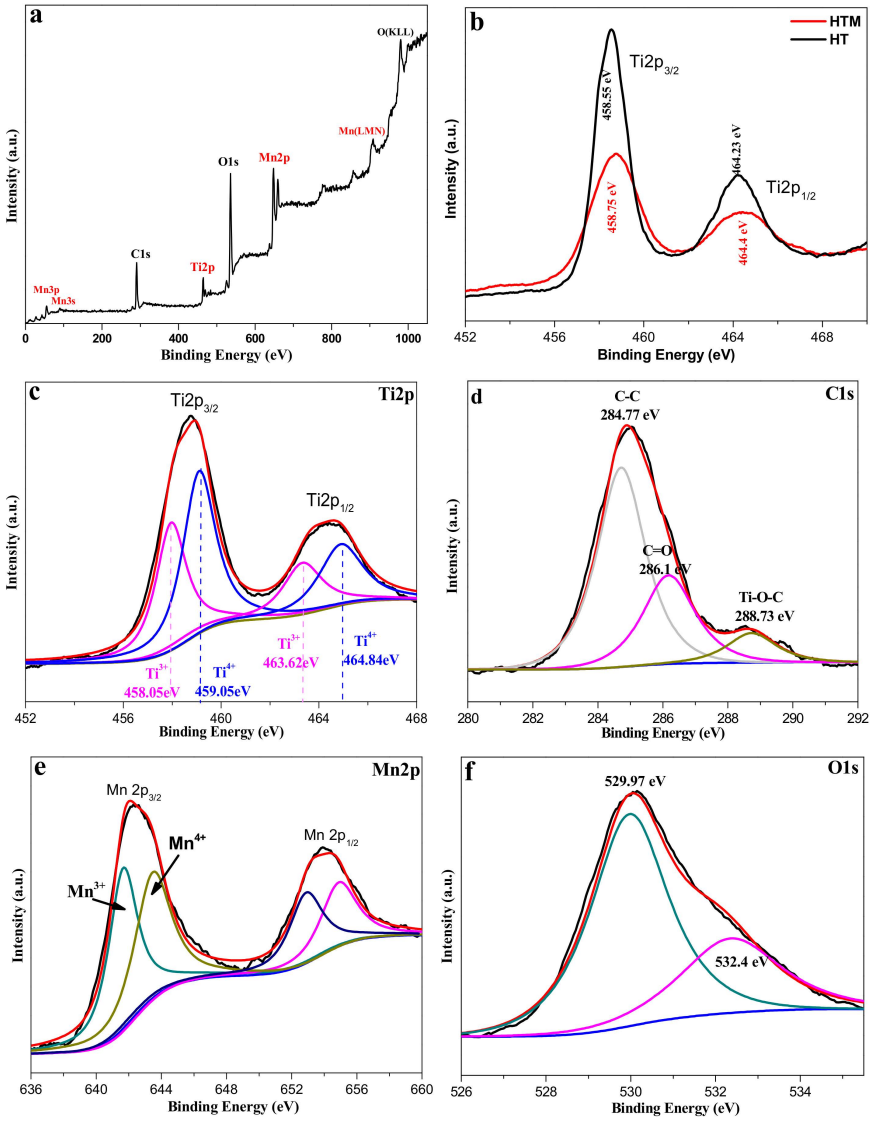

Figure 5. XPS fully scanned spectrum of HTM (**a**), XPS spectra of Ti2p (**b**), Ti2p Gaussian peaks (**c**), C1s (**d**), O1s (**e**), Mn2p (**f**).

Figure 5d shows that the C1s spectrum of the HTM sphere can be fitted to three different peaks of 284.77, 286.1 and 288.73 eV, indicating that there are three carbon chemical environments in the

HTM spheres. The peak at 284.77 eV is assigned to the existence of vestigial carbon, which serves as an adsorbent for organic pollutants and as a photo-sensitizer to drive the faster degradation of pollutants [9]. As demonstrated in Figure 5e and Table S1, two distinct peaks located at 642 and 653.8 eV can be ascribed to $Mn2p_{3/2}$ and $Mn2p_{1/2}$, respectively [39]. The energy separation between $Mn2p_{3/2}$ and $Mn2p_{1/2}$ is about 11.8 eV, which is a typical value for MnO_2 [39,40]. Figure 5f shows the XPS spectrum of O1s, there is a peak at 529.97 eV related to the bulk oxygen bound of TiO_2. In addition, the peak at 532.1 eV is responsible for hydroxyl groups adsorbed onto the surface of TiO_2 [9,10].

2.3. Catalytic Activity of HTM Spheres

2.3.1. Chemical Oxidation Activity of HTM

Under the existence of oxone (PMS), the chemical oxidation performance of as-synthesized HTM was investigated by degrading phenol. The commercial active MnO_2 (CAM) and hollow TiO_2 spheres (HT) were used as reference materials. Figure 6 suggests that the removal rate of phenol is negligible after the addition of PMS, suggesting that phenol is extremely hard to be degraded under only the existence of an oxidant because there is no thermal activation of Oxone for the production of sulfate radicals [2,24]. Similarly, hollow TiO_2 spheres (HT) with a high surface area (~90.2283 m^2/g) also cannot degrade phenol by adding PMS without light irradiation. For commercial active MnO_2 (CAM), the degradation rate of phenol is as low as 18% under PMS. By contrast, the removal rate of phenol is as high as 92% under the same oxidation conditions for the as-synthesized HTM hollow spheres because its large surface-to-volume ratio (HTM: 53.7827 m^2/g; MnO_2 (Figure S4): 25.7805 m^2/g) and hollow/porous characteristics facilitate the access of reactant phenol molecules [30,37]. Unfortunately, even if the PMS is added again after 60 min (Figure S5), the removal of phenol does not increase accordingly. In addition, a longer oxidation times does not result in a higher degradation rate of phenol for the as-synthesized HTM, indicating the incomplete removal of phenol, as reported in many previous publications [2,19,23,25]. Therefore, further degradation is very necessary for the complete removal of phenol.

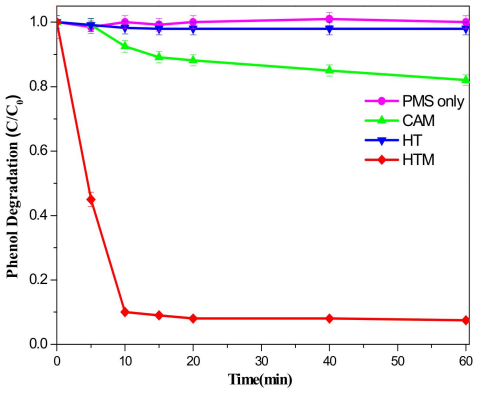

Figure 6. Chemical oxidation activity of different materials for phenol removal.

2.3.2. Photo-Degradation Activity of HTM

As afore-mentioned, the complete removal of phenol is very difficult in using only the chemical oxidation ability of MnO_2 in the HTM sample. Gratifyingly, the as-synthesized HTM also holds strong photocatalytic activity due to the modification of the electronic energy band structure of TiO_2 through the coating of MnO_2 [30]. Figure S6 shows that HTM exhibits strong light absorption in the region of 200–750 nm due to MnO_2 coverage, narrowing the band gap (~2.86 eV) of TiO_2, as shown in Figure S6b [30]. After the chemical oxidation (60 min), the second stage of the photo-degradation experiment was further carried out under simulated solar light radiation. Figure 7 indicates that the removal rate of phenol further increases with the increase in irradiation time, suggesting that HTM

exhibits a photo-degradation activity for phenol. Excitedly, the complete degradation of phenol can be achieved after 180 min irradiation, effectively overcoming the incomplete degradation of phenol for hollow TiO_2 and MnO_2 (Figure S7).

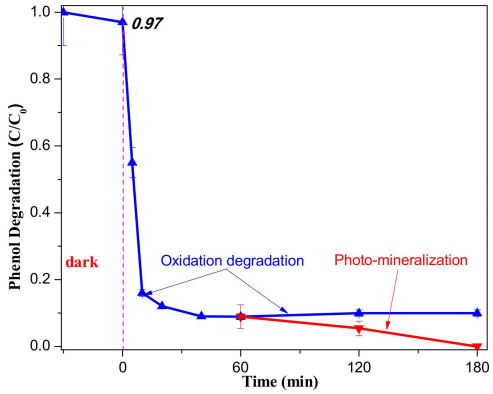

Figure 7. Phenol removal under chemical oxidation–degradation and photo-mineralization.

2.3.3. Total Organic Carbon (TOC) Measurement

Total organic carbon (TOC) measurement has been widely used to assess the mineralization of organic pollutants [2,19]. TOC removal profiles for phenol degradation on HTM hollow spheres are presented in Figure 8. As seen, the as-synthesized HTM with or without simulated sunlight irradiation exhibits TOC reduction of phenol under the presence of oxidant PMS in a short time. Only under PMS, the HTM provides excellent phenol mineralization capabilities and more than 91% of TOC (Table S2) is removed and transfers into inorganic carbon forms within 60 min. However, 100% of TOC reduction is not able to be achieved even when the oxidation time is prolonged to 180 min, indicating the incomplete mineralization of phenol for HTM. Excitedly, an enhanced TOC reduction of phenol is observed after simulated solar light irradiation, and 100% of TOC reduction is obtained when the irradiation time is prolonged to 180 min, strongly suggesting that a small quantity of residual phenol and intermediates can be completely removed by the photo-degradation stage. The order of the TOC removal fairly agrees with the order of the two stages of degradation reaction rates on HTM hollow spheres.

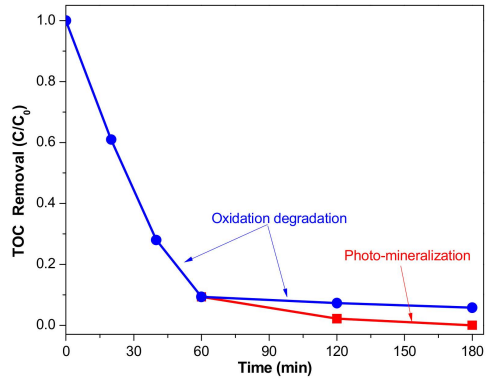

Figure 8. TOC removal profiles during phenol degradation.

2.4. Mineralization Mechanism and Pathway of Phenol

To expound the complete mineralization of phenol for HTM hollow spheres, a probable degradation-mechanism is proposed based on the hierarchically-structured TiO_2/MnO_2, as shown in Figure 9a. In the first stage, a MnO_2 shell in the HTM sample can activate PMS to generate lots of sulfate radicals ($SO^{4-}\bullet$) [19,24], subsequently, the generated sulfate radicals rapidly react with phenol in a short time (60 min), leading to the fast degradation of phenol (91%). However, the higher

removal of phenol cannot be obtained even when the oxidation time is further prolonged to 180 min, which is mainly ascribed to the low concentration of phenol after oxidation degradation and extremely low adsorption amount of phenol (~3%) obtained by referring to our previous method [10], significantly decreasing the reaction with phenol and resulting in a negligibly enhanced removal of phenol. This is why the incomplete mineralization of phenolic compounds is reported in many previous publications [2,19,23,25]. In the second stage, inner TiO_2 in the HTM sample is easy to activate under simulated solar light irradiation and generates numerous electron/hole pairs [9]. The dissolved O_2 easily traps photo-generated electrons [41], forming superoxide radical ($\bullet O^{2-}$), in which $\bullet O^{2-}$ is a crucial active specie for mineralizing residual phenol and its intermediates because dissolved O_2 can participate in the photo-degradation process through the porous channels and reaction medium (water) [42], resulting in the complete mineralization of phenol.

To obtain the possible degradation pathway of phenol, the transformation intermediates were detected by MS during the degradation process, as shown in Figure 9b. The product with m/z = 94.09 is attributed to the molecular weight of phenol. Two possible degradation pathways of phenol are proposed in this study. After sulfate radicals and hydroxyl radicals are generated by activating PMS under MnO_2, phenol is attacked by the radicals, generating phenol radicals. Subsequently, the phenol radical is further attacked to produce p-hydroxybenzoic acid with m/z = 139.96 or a small amount of pyrocatechol with m/z = 109.05. Finally, these intermediates undergo further degradation under radicals or light irradiation to produce CO_2 and H_2O.

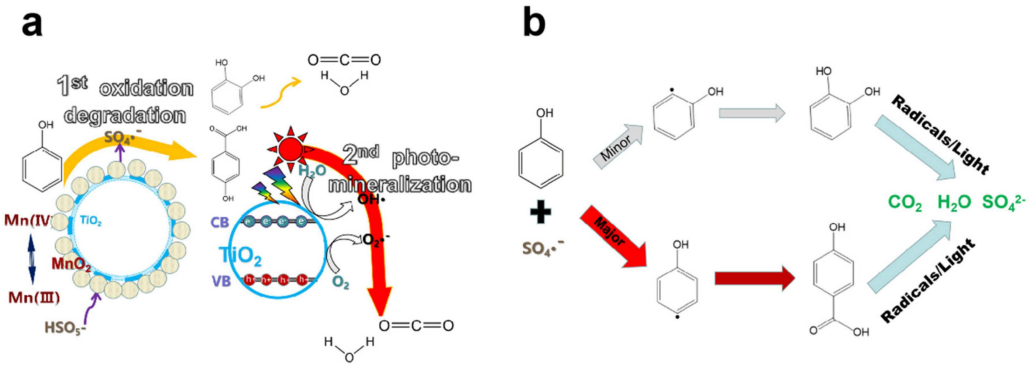

Figure 9. Proposed mechanism (**a**) and pathway (**b**) of phenol degradation for as-synthesized HTM hollow spheres.

2.5. Recyclability of HTM Spheres

Recyclability is an important factor for the practical application of HTM. After each degradation test, the HTM sample was centrifuged, rinsed, dried, and reused for the next run. Figure 10a illustrates the performance of HTM towards the degradation of phenol. As seen, the HTM can still be used with the order of the two stages of phenol removal even after three recycling runs, implying that the HTM possess a good stability (Figure S8) for the mineralization of phenol in wastewater. Clearly, the enhanced catalytic performance of the HTM has been associated with the changes in their structural and optical properties [26]. To further understand the action of TiO_2 and MnO_2, we prepared MnO_2 without a hollow TiO_2 template by using the same method [43]. Accordingly, MnO_2 and hollow TiO_2 spheres (HT) were used for the degradation of phenol. Figure 10b indicates that MnO_2 and HT both exhibit a lower removal rate of phenol than the HTM. Particularly, MnO_2 does not enhance the degradation rate of phenol even under simulated solar light irradiation; by contrast, an enhanced removal of phenol is observed by HT, yet below the mineralization of phenol for as-synthesized HTM. Moreover, poor recyclability is found for MnO_2 and HT. The results strongly confirm that the as-synthesized HTM exhibits a complete removal of phenol and good recyclability, substantially broadening its practical potential.

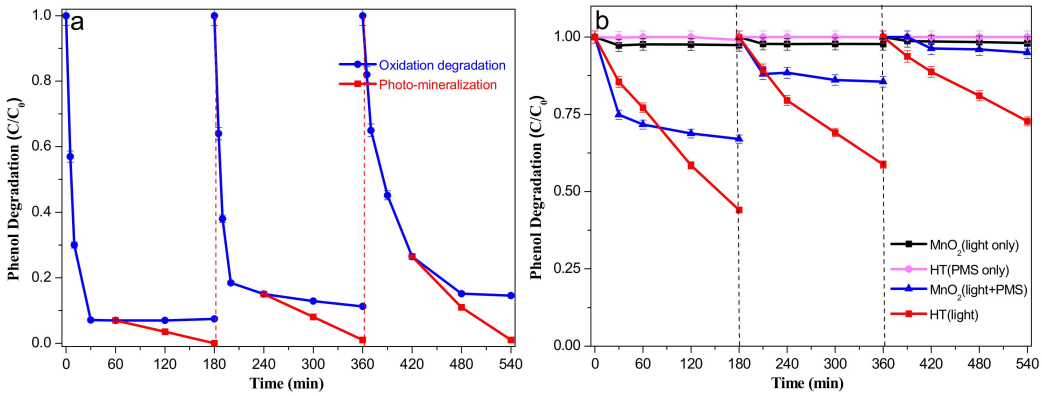

Figure 10. Recyclability of HTM spheres (**a**) and HT and MnO_2 (**b**) for phenol degradation.

3. Materials and Methods

3.1. Materials

Chemicals including methacryloyloxyethyltrimethylammonium chloride (DMC), potassium persulfate ($K_2S_2O_8$), hexadecyl trimethyl ammonium bromide (CTAB), and Titaniumtetrabutoxide (TBT) were available from J&K Chemical Technology (Shanghai, China). Commercially activated manganese dioxide (CAM: analytical reagent, 85%, Figure S9), Oxone® ($2KHSO_5 \cdot KHSO_4 \cdot K_2SO_4$, PMS) were obtained from Macklin Biochemical Co. Ltd. (Shanghai, China) Styrene (St), phenol (99%), manganese nitrate and anhydrous ethanol were purchased from the Sinopharm Chemical Reagent Co. Ltd. (Shanghai, China), in which styrene was purified by using a NaOH solution.

3.2. Preparation of TiO_2 Spheres

Hollow TiO_2 spheres (HT) were synthesized via the following steps: firstly, cationic polystyrene spheres (CPS) were developed by referring to our previous works [10,28,44]. Secondly, the CPS spheres were dispersed in absolute ethanol at 0 °C and then TBT ethanol solution was slowly added into the reaction system. After that, the reaction medium was further maintained for 24 h in order that that TBT hydrolysate be adsorbed on the surface of CPS via electronic attraction. Thirdly, a mixture of deionized water and ethanol was dropped into the system to form CPS@TiO_2 particles. Finally, the resulting CPS@TiO_2 was filtered, washed repeatedly and calcined at 450 °C to prepare hollow TiO_2 spheres.

3.3. Preparation of TiO_2/MnO_2 (HTM) Spheres

The as-synthesized hollow TiO_2 spheres (1.0 g) were further dispersed in ethanol solution (50 mL). Manganese nitrate (2.0 g) ethanol solution (20 mL) was slowly added into the reaction system via a syringe. The system was kept at 0 °C for 12 h. Subsequently, the solution was evaporated at 70 °C by referring to previous publication [43]. Finally, TiO_2/MnO_2 (HTM) spheres were obtained after calcination at 450 °C for 6 h.

3.4. Characterization

The internal and external morphology of TiO_2 and HTM spheres were measured by a field emission scanning electron microscope (JEOL, Tokyo, Japan, JSM-7001F, 10.00 KV) and a high-resolution transmission electron microscope (JEOL JEM-2100, 200 KV). Specific surface area and pore size distribution of the TiO_2 and HTM spheres were determined by Tristar 3020II (Micromeretics, Norcross, GA, USA). The crystal structure of the HTM spheres were investigated by X-ray diffractometer (Bruker D8 Advance) using Cu-Kα radiation at 40 kV and 40 mA (20°–80°). In addition, the bond energy of the HTM spheres were measured by X-ray photoelectron spectroscopy (Thermo ESCALAB 250Xi). UV-vis spectroscopy was tested by UV2600 (Hitach, Tokyo, Japan). Total organic carbon (TOC) was determined using a Shimadzu TOC-L_{cph} analyzer for selected samples.

3.5. Activity Measurement

The activity measurement of HTM was investigated by degrading phenol solution. In the first stage, the oxidation activity of HTM was carried out at 25 °C for the degradation of phenol. At first, 20 mg of the HTM sphere was added to the phenol solution (5 mg/L, 50 mL) for 30 min to reach the adsorption-desorption equilibrium [2]. Secondly, PMS (0.025 g) was added into the phenol solution for starting the oxidation of phenol. After 60 min oxidation-degradation, the second stage of photo-mineralization was further conducted under simulated solar light irradiation (XHA 300 W Xe lamp with an AM 1.5 G filter) to realize the complete mineralization of phenol [9]. The resulting sample (5 mL) was taken out from the reactive system, and was then quenched [45], filtered and analyzed by UV-vis spectrum (λ = 270 nm) [24]. Incidentally, the reported value is an average value of three measurements. For the recyclability test, the HTM sample was recycled by filtrating, washed with deionized water after each run, and dried at 60 °C for 12 h [2]. In addition, the degradation behaviors of phenol for homemade MnO_2 with a narrow size range (Figure S10) was conducted under the same conditions.

4. Conclusions

In summary, we have devised a hierarchically-structured TiO_2/MnO_2 hollow sphere. During the removal process of phenol, HTM can fully exert their respective advantages in the TiO_2 and MnO_2 species, realizing the first stage of the rapid oxidation degradation of phenol and the second stage of the complete photo-mineralization of residual phenol and its intermediates. TOC measurement confirms that HTM can achieve the complete removal of phenol, efficiently overcoming the incomplete mineralization of phenolic compounds for many previously reported TiO_2 or MnO_2-based materials. Therefore, this work provides a new insight in constructing hierarchically-structured hollow spheres with two or more species, achieving the complete mineralization of refractory organic compounds.

Supplementary Materials: The following are available online at http://www.mdpi.com/2073-4344/9/4/390/s1. Figure S1: TGA and DSC curves of HTM spheres; Figure S2: Raman spectra of HTM spheres; Figure S3: Selected electron area diffraction of HTM spheres; Table S1: the parameters of Ti and Mn in XPS spectrum for HTM sample; Figure S4: N2 adsorption-desorption isotherms and pore size distribution (insert) of CAM; Figure S5: Effect of oxidant on the degradation of Phenol for HTM; Figure S6: (a) UV-vis absorption spectra of HTM and hollow TiO2 spheres (b) Band gap energy (Eg) of HTM and hollow TiO2 spheres; Figure S7: Degradation of phenol for hollow TiO2 photocatalyst and MnO2; Table S2: Comparative degradation rate of various catalysts. Figure S8: TEM image of HTM after cycles Figure S9: SEM of CAM; Figure S10: Particle distribution of as-synthesized MnO2 nanoparticles.

Author Contributions: Investigation, C.J., and S.C.; Data Curation, C.J. and W.C.; Writing—Original Draft Preparation, C.J. and S.C.; Writing—Review & Editing, Y.G., and H.L.; formal analysis: Y.G., L.H. and Y.Z. Funding Acquisition, L.H. and S.C.

Funding: Financial support of this research from the National Natural Science Foundation of China (Grants 21876069) and the Natural Science Foundation (1608085MB34, KJ2017ZD28, gxgwfx2018059) in Anhui Province of China.

Conflicts of Interest: The authors declare no conflict of interest.

References

1. Taran, O.P.; Ayusheev, A.B.; Ogorodnikova, O.L.; Prosvirin, I.P.; Isupova, L.A.; Parmon, V.N. Perovskite-like catalysts $LaBO_3$ (B = Cu, Fe, Mn, Co, Ni) for wet peroxide oxidation of phenol. *Appl. Catal. B Environ.* **2016**, *180*, 86–93. [CrossRef]
2. Wang, Y.; Sun, H.; Ang, H.M.; Tadé, M.O.; Wang, S. 3D-hierarchically structured MnO_2 for catalytic oxidation of phenol solutions by activation of peroxymonosulfate: Structure dependence and mechanism. *Appl. Catal. B Environ.* **2015**, *164*, 159–167. [CrossRef]
3. Wei, Z.; Liang, F.; Liu, Y.; Luo, W.; Wang, J.; Yao, W.; Zhu, Y. Photoelectrocatalytic degradation of phenol-containing wastewater by TiO_2/gC_3N_4 hybrid heterostructure thin film. *Appl. Catal. B Environ.* **2017**, *201*, 600–606. [CrossRef]

4. Liang, F.; Zhu, Y. Enhancement of mineralization ability for phenol via synergetic effect of photoelectrocatalysis of g-C_3N_4 film. *Appl. Catal. B Environ.* **2016**, *180*, 324–329. [CrossRef]
5. Huang, Y.; Pinar, C.; Lai, T.; Yu, P. Phenol removal from water by polyamide and AgCl mineralized thin-film composite forward osmosis membranes. *Ind. Eng. Chem. Res.* **2018**, *57*, 7021–7029. [CrossRef]
6. Hasanoğlu, A. Removal of phenol from wastewaters using membrane contactors: Comparative experimental analysis of emulsion pertraction. *Desalination* **2013**, *309*, 171–180. [CrossRef]
7. Turki, A.; Guillard, C.; Dappozze, F.; Ksibi, Z.; Berhault, G.; Kochkar, H. Phenol photocatalytic degradation over anisotropic TiO_2 nanomaterials: Kinetic study, adsorption isotherms and formal mechanisms. *Appl. Catal. B Environ.* **2015**, *163*, 404–414. [CrossRef]
8. Murcia, J.J.; Hidalgo, M.C.; Navío, J.A.; Araña, J.; Doña-Rodríguez, J.M. Study of the phenol photocatalytic degradation over TiO_2 modified by sulfation, fluorination, and platinum nanoparticles photodeposition. *Appl. Catal. B Environ.* **2015**, *179*, 305–312. [CrossRef]
9. Gao, D.; Yu, H.; Xu, Y. Direct photoinduced synthesis and high H_2-evolution performance of Bi-modified TiO_2 photocatalyst in a Bi(III)-EG complex system. *Appl. Surf. Sci.* **2018**, *462*, 623–632. [CrossRef]
10. Shao, J.; Sheng, W.; Wang, M.; Li, S.; Chen, J.; Zhang, Y.; Cao, S. In situ synthesis of Carbon-doped TiO_2 single-crystal nanorods with a Remarkably photocatalytic efficiency. *Appl. Catal. B Environ.* **2017**, *209*, 311–319. [CrossRef]
11. Cheng, L.; Qiu, S.; Chen, J.; Shao, J.; Cao, S. A practical pathway for the preparation of Fe_2O_3 decorated TiO_2 photocatalyst with enhanced visible-light photoactivity. *Mater. Chem. Phys.* **2017**, *190*, 53–61. [CrossRef]
12. Makrigianni, V.; Giannakas, A.; Daikopoulos, C.; Deligiannakis, Y.; Konstantinou, I. Preparation, characterization and photocatalytic performance of pyrolytic-tire-char/TiO_2 composites, toward phenol oxidation in aqueous solutions. *Appl. Catal. B Environ.* **2015**, *175*, 244–252. [CrossRef]
13. Wang, J.; He, B.; Kong, X.Z. A study on the preparation of floating photocatalyst supported by hollow TiO_2 and its performance. *Appl. Surf. Sci.* **2015**, *327*, 406–412. [CrossRef]
14. Zheng, Q.; Lee, H.J.; Lee, J.; Choi, W.; Park, N.B.; Lee, C. Electrochromic titania nanotube arrays for the enhanced photocatalytic degradation of phenol and pharmaceutical compounds. *Chem. Eng. J.* **2014**, *249*, 285–292. [CrossRef]
15. Li, H.; Ji, J.; Cheng, C.; Liang, K. Preparation of phenol-formaldehyde resin-coupled TiO_2 and study of photocatalytic activity during phenol degradation under sunlight. *J. Phys. Chem. Solids* **2018**, *122*, 25–30. [CrossRef]
16. Shi, B.N.; Wan, J.F.; Liu, C.T.; Yu, X.J.; Ma, F.W. Synthesis of $CoFe_2O_4$/MCM-41/TiO_2 composite microspheres and its performance in degradation of phenol. *Mater. Sci. Semicond. Process.* **2015**, *37*, 241–249. [CrossRef]
17. Saputra, E.; Muhammad, S.; Sun, H.; Patel, A.; Shukla, P.; Zhu, Z.H.; Wang, S. α-MnO_2 activation of peroxymonosulfate for catalytic phenol degradation in aqueous solutions. *Catal. Commun.* **2012**, *26*, 144–148. [CrossRef]
18. Luo, S.; Lian, D.; Sun, B.; Wei, M.; Li, X.; Xu, A. Manganese oxide octahedral molecular sieve (OMS-2) as an effective catalyst for degradation of organic dyes in aqueous solutions in the presence of peroxymonosulfate. *Appl. Catal. B Environ.* **2015**, *164*, 92–99. [CrossRef]
19. Wang, Y.; Indrawirawan, S.; Duan, X.; Sun, H.; Ang, H.M.; Tadé, M.O.; Wang, S. New insights into heterogeneous generation and evolution processes of sulfate radicals for phenol degradation over one-dimensional α-MnO_2 nanostructures. *Chem. Eng. J.* **2015**, *266*, 12–20. [CrossRef]
20. Jie, L.; Zhao, Z.; Shao, P.; Cui, F. Activation of peroxymonosulfate with magnetic Fe_3O_4–MnO_2 core–shell nanocomposites for 4-chlorophenol degradation. *Chem. Eng. J.* **2015**, *262*, 854–861.
21. Khan, A.; Liao, Z.; Yong, L.; Jawad, A.; Ifthikar, J.; Chen, Z. Synergistic degradation of phenols using peroxymonosulfate activated by CuO-Co_3O_4 @MnO_2 nanocatalyst. *J. Hazard. Mater.* **2017**, *329*, 262–271. [CrossRef] [PubMed]
22. Wang, Y.; Xie, Y.; Sun, H.; Xiao, J.; Cao, H.; Wang, S. 2D/2D nano-hybrids of γ-MnO_2 on reduced graphene oxide for catalytic ozonation and coupling peroxymonosulfate activation. *J. Hazard. Mater.* **2016**, *301*, 56–64. [CrossRef] [PubMed]
23. Liang, H.; Sun, H.; Patel, A.; Shukla, P.; Zhu, Z.H.; Wang, S. Excellent performance of mesoporous Co_3O_4/MnO_2 nanoparticles in heterogeneous activation of peroxymonosulfate for phenol degradation in aqueous solutions. *Appl. Catal. B Environ.* **2012**, *127*, 330–335. [CrossRef]

24. Saputra, E.; Muhammad, S.; Sun, H.; Ang, H.M.; Wang, S. Different crystallographic one-dimensional MnO_2 nanomaterials and their superior performance in catalytic phenol degradation. *Environ. Sci. Technol.* **2013**, *47*, 5882–5887. [CrossRef]
25. Saputra, E.; Zhang, H.; Liu, Q.; Sun, H.; Wang, S. Egg-shaped core/shell α-Mn_2O_3@α-MnO_2 as heterogeneous catalysts for decomposition of phenolics in aqueous solutions. *Chemosphere* **2016**, *159*, 351. [CrossRef] [PubMed]
26. López, M.; Lemus, M.; Hidalgo, M.; González, R.; Owen, P.; Oros-Ruiz, S.; López, S.; Acosta, J. Synthesis and Characterization of ZnO-ZrO_2 Nanocomposites for Photocatalytic Degradation and Mineralization of Phenol. *J. Nanomater.* **2019**, *12*, 1015876.
27. Zhao, S.; Chen, J.; Liu, Y.; Jiang, Y.; Jiang, C.; Yin, Z.; Xiao, Y.; Cao, S. Silver nanoparticles confined in shell-in-shell hollow TiO_2 manifesting efficiently photocatalytic activity and stability. *Chem. Eng. J.* **2019**, *367*, 249–259. [CrossRef]
28. Cao, S.; Chang, J.; Fang, L.; Wu, L. Metal nanoparticles confined in the nanospace of double-shelled hollow silica spheres for highly efficient and selective catalysis. *Chem. Mater.* **2016**, *28*, 5596–5600. [CrossRef]
29. Dharmarathna, S.; King'Ondu, C.K.; Pahalagedara, L.; Kuo, C.H.; Zhang, Y.; Suib, S.L. Manganese octahedral molecular sieve (OMS-2) catalysts for selective aerobic oxidation of thiols to disulfides. *Appl. Catal. B Environ.* **2014**, *147*, 124–131. [CrossRef]
30. Xue, M.; Huang, L.; Wang, J.; Wang, Y.; Gao, L.; Zhu, J.; Zou, Z. The direct synthesis of mesoporous structured MnO_2/TiO_2 nanocomposite: A novel visible-light active photocatalyst with large pore size. *Nanotechnology* **2008**, *19*, 185604. [CrossRef]
31. Zhang, Y.; Chen, J.; Tang, H.; Xiao, Y.; Qiu, S.; Li, S.; Cao, S. Hierarchically-structured SiO_2-Ag@TiO_2 hollow spheres with excellent photocatalytic activity and recyclability. *J. Hazard. Mater.* **2018**, *354*, 17–26. [CrossRef] [PubMed]
32. Shin, D.; Shin, J.; Yeo, T.; Hwang, H.; Park, S.; Choi, W. Scalable Synthesis of Triple-Core–Shell Nanostructures of TiO_2@MnO_2@C for High Performance Supercapacitors Using Structure-Guided Combustion Waves. *Small* **2018**, *14*, 1703755. [CrossRef]
33. Li, B.; Zhao, Z.; Gao, F.; Wang, X.; Qiu, J. Mesoporous microspheres composed of carbon-coated TiO_2 nanocrystals with exposed {0 0 1} facets for improved visible light photocatalytic activity. *Appl. Catal. B Environ.* **2014**, *147*, 958–964. [CrossRef]
34. Braun, A.; Akurati, K.K.; Fortunato, G.; Reifler, F.A.; Ritter, A.; Harvey, A.S.; Vital, A.; Graule, T. Nitrogen doping of TiO_2 photocatalyst forms a second eg state in the Oxygen(1s) NEXAFS pre-edge. *Physics* **2016**, *114*, 516–519. [CrossRef]
35. Li, Y.; Wang, G.; Ye, K.; Cheng, K.; Pan, Y.; Yan, P.; Yin, J.; Cao, D. Facile preparation of three-dimensional multilayer porous MnO_2/reduced graphene oxide composite and its supercapacitive performance. *J. Power Sources* **2014**, *271*, 582–588. [CrossRef]
36. Yu, P.; Zhang, X.; Chen, Y.; Ma, Y. Solution-combustion synthesis of ε-MnO_2 for supercapacitors. *Mater. Lett.* **2010**, *64*, 61–64. [CrossRef]
37. Ghosh, M.; Liu, J.; Chuang, S.S.C.; Jana, S.C. Fabrication of Hierarchical V2O5 Nanorods on TiO_2 Nanofibers and Their Enhanced Photocatalytic Activity under Visible Light. *ChemCatChem* **2018**, *10*, 3305–3318. [CrossRef]
38. Zhang, Y.; Chen, J.; Hua, L.; Li, S.; Zhang, X.; Sheng, W.; Cao, S. High photocatalytic activity of hierarchical SiO_2@C-doped TiO_2 hollow spheres in UV and visible light towards degradation of rhodamine B. *J. Hazard. Mater.* **2017**, *340*, 309–318. [CrossRef]
39. Huang, L.; Hu, X.; Yuan, S.; Li, H.; Yan, T.; Shi, L.; Zhang, D. Photocatalytic preparation of nanostructured MnO_2-(Co_3O_4)/TiO_2 hybrids: The formation mechanism and catalytic application in SCR deNOx reaction. *Appl. Catal. B Environ.* **2017**, *203*, 778–788. [CrossRef]
40. Yu, N.; Yin, H.; Zhang, W.; Liu, Y.; Tang, Z.; Zhu, M.Q. High-performance fiber-shaped all-solid-state asymmetric supercapacitors based on ultrathin MnO_2 nanosheet/carbon fiber cathodes for wearable electronics. *Adv. Energy Mater.* **2016**, *6*, 1501458. [CrossRef]
41. Yu, S.; Yun, H.J.; Yong, H.K.; Yi, J. Carbon-doped TiO_2 nanoparticles wrapped with nanographene as a high performance photocatalyst for phenol degradation under visible light irradiation. *Appl. Catal. B Environ.* **2014**, *144*, 893–899. [CrossRef]

42. Li, M.; Yu, J.; Fei, H.; Ling, J.; Wu, Y.; Yang, L.; Han, X.; Ying, L.; Liu, A.; Wei, W. Boosting gas involved reactions at nanochannel reactor with joint gas–solid–liquid interfaces and controlled wettability. *J. Am. Chem. Soc.* **2017**, *139*, 10441.
43. Bai, B.; Li, J.; Hao, J. 1D-MnO_2, 2D-MnO_2 and 3D-MnO_2 for low-temperature oxidation of ethanol. *Appl. Catal. B Environ.* **2015**, *164*, 241–250. [CrossRef]
44. Zhang, Y.; Zhao, Y.; Cao, S.; Yin, Z.; Cheng, L.; Wu, L. Design and synthesis of hierarchical SiO_2@C/TiO_2 hollow spheres for high-performance supercapacitors. *ACS Appl. Mater. Interfaces* **2017**, *9*, 29982–29991. [CrossRef] [PubMed]
45. Shi, W.; Guo, F.; Yuan, S. In situ synthesis of Z-scheme Ag_3PO_4/$CuBi_2O_4$ photocatalysts and enhanced photocatalytic performance for the degradation of tetracycline under visible light irradiation. *Appl. Catal. B Environ.* **2017**, *209*, 720–728. [CrossRef]